ACS APPLIED MATERIALS & INTERFACES

Research Article

www.acsami.org

$CoNi_2S_4$ Nanosheet Arrays Supported on Nickel Foams with Ultrahigh Capacitance for Aqueous Asymmetric Supercapacitor Applications

Wei Hu, Ruqi Chen, Wei Xie, Lilan Zou, Ni Qin, and Dinghua Bao*

State Key Laboratory of Optoelectronic Materials and Technologies, School of Physics and Engineering, Sun Yat-Sen University, Guangzhou 510275, China

Supporting Information

ABSTRACT: We report that $CoNi_2S_4$ nanosheet arrays exhibit ultrahigh specific capacitance of 2906 F g^{-1} and areal capacitance of 6.39 F cm^{-2} at a current density of 5 mA cm^{-2}, as well as good rate capability and cycling stability, and superior electrochemical performances with an energy density of 33.9 Wh kg^{-1} at a power density of 409 W kg^{-1} have been achieved in an assembled aqueous asymmetric supercapacitor. The $CoNi_2S_4$ nanosheet arrays were in situ grown on nickel foams by a facile two-step hydrothermal method. The formation mechanism of the $CoNi_2S_4$ nanosheet arrays was based on an anion-exchange reaction involving the pseudo Kirkendall effect. The two aqueous asymmetric supercapacitors in series using the $CoNi_2S_4$ nanosheet arrays as the positive electrodes can power four 3-mm-diameter red-light-emitting diodes. The outstanding supercapacitive performance of $CoNi_2S_4$ nanosheet arrays can be attributed to ravine-like nanosheet architectures with good mechanical and electrical contact, low crystallinity and good wettability without an annealing process, rich redox reactions, as well as high conductivity and transport rate for both electrolyte ions and electrons. Our results demonstrate that $CoNi_2S_4$ nanosheet arrays are promising electrode materials for supercapacitor applications.

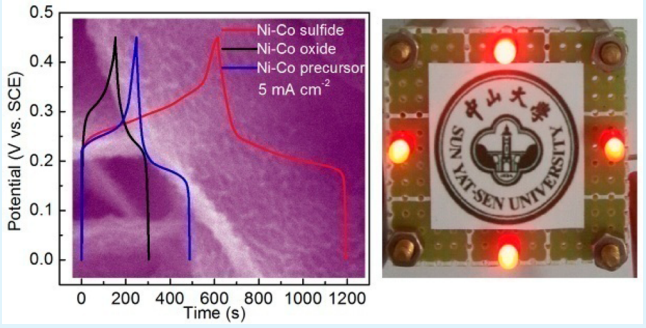

KEYWORDS: *$CoNi_2S_4$, nanosheet arrays, anion-exchange reaction, supercapacitor, energy storage*

1. INTRODUCTION

Recently, urgent and increasing demands for clean, efficient, and sustainable energy have greatly stimulated substantial research on alternative energy storage and conversion. Among the effective and practical technologies for energy storage and conversion, supercapacitors, also called electrochemical capacitors, have been considered as one of the most promising energy-storage devices and wildly investigated for applications in portable electronic devices and electric vehicles because of their advantages such as fast charge−discharge process, high power density, and long cycle life.[1−4] Generally, electrochemical capacitors have been divided into two types in terms of the charge-storage mechanism. One is an electrochemical double-layer capacitor (EDLC), which is dominated by electrostatic charge diffusion and accumulation at the interface of the carbon electrode and electrolyte. The carbon-based electrode materials (e.g., active carbon, carbon nanotubes, and graphene) exhibit excellent conductivity and chemical stability.[4−6] However, the carbon-based electrodes suffer from relatively low specific capacitance.[6,7] The other one, in contrast, is a pseudocapacitor, which is mainly dominated by reversible fast surface Faradaic redox reactions and can provide much higher specific capacitance than EDLC.[3,7,8]

Transition-metal oxides, hydroxides, and conducting polymers are demonstrated in supercapacitor applications based on their pseudocapacitive properties.[7−11] More recently, metal sulfides have attracted extensive attention owing to their excellent potential applications in optics, catalysis, sensing, solar energy, and batteries.[12] Furthermore, metal sulfides are also especially notable candidates for pseudocapacitors because of their low electronegativity and high electrochemical activity.[13−17] Several metal sulfides can be easily synthesized by a facile and effective hydrothermal anion-exchange reaction method. Pu et al. prepared Co_9S_8 nanotube arrays supported on nickel foam for a high-performance supercapacitor.[13] Xia et al. synthesized NiS, Co_9S_8, CoS, and CoS/NiS nanostructures for electrochemical energy storage.[14] Besides, it has been proven that Ni−Co sulfides have much lower optical band-gap energy and higher conductivity compared to Ni−Co oxides.[18] The substitution of oxygen with sulfur could create a more flexible structure because the electronegativity of sulfur is lower than that of oxygen.[19] In addition, ternary Ni−Co sulfides possess richer redox reaction and higher electronic conductivity

Received: August 11, 2014
Accepted: October 16, 2014
Published: October 16, 2014

 © 2014 American Chemical Society

compared with binary metal sulfides including NiS, CoS, and Co_9S_8.[15,20] Various morphologies and structures of Ni−Co sulfides, such as $NiCo_2S_4$ nanotubes,[15−17] $NiCo_2S_4$ urchin-like nanostructures,[18] Ni−Co sulfide nanowires,[20] $NiCo_2S_4$ nanonetworks,[21] shape-controlled $NiCo_2S_4$,[22] $CoNi_2S_4$ mushroom-like arrays,[23] and $Ni_xCo_{3-x}S_4$ hollow nanoprisms,[24] have been obtained to investigate the supercapacitive performance. For instance, Peng et al. have synthesized $NiCo_2S_4$ nanosheets on graphene with high capacitance and long cycle life.[25] Chen et al. have in situ fabricated $NiCo_2S_4$ nanotube arrays on nickel foam to achieve ultrahigh areal capacitance.[15]

High-performance supercapacitor electrodes should display characteristics such as high utilization efficiency and high mass loading of electroactive materials as well as high transport rate for both electrolyte ions and electrons. Thus, it is of significance to prepare high mass loading active materials directly through mechanical and electrical contact with the current collector for improved supercapacitor performance. It has been reported that $CoNi_2S_4$ nanoparticles,[26] $CoNi_2S_4$/graphene nanocomposites[27] with additive binder, and $CoNi_2S_4$ mushroom-like arrays[23] on nickel foam as supercapacitor electrodes. However, there is no report on $CoNi_2S_4$ nanosheet arrays directly deposited on nickel foams for supercapacitor applications. It is expected that $CoNi_2S_4$ nanosheet arrays grown directly on nickel foams can lead to superior pseudocapacitive performance. In this work, using a facile two-step hydrothermal method, we have successfully in situ synthesized $CoNi_2S_4$ nanosheet arrays on nickel foams. The as-fabricated $CoNi_2S_4$ nanosheet arrays manifest ultrahigh specific and areal capacitance values as well as good cycling stability. The assembled aqueous asymmetric supercapacitor cell exhibits high energy density and power density. Our results suggest that the $CoNi_2S_4$ nanosheet arrays can act as high-performance electrode materials for supercapacitor applications.

2. EXPERIMENTAL SECTION

2.1. Materials Preparation. All of the reagents were analytical grade and were used without further purification. Before the deposition of Ni−Co precursor on nickel foam, the nickel foam was immersed in a 3 M HCl solution for 10 min to remove the possible surface oxide layer and cleaned sequentially in ethanol and deionized water for 15 min, respectively.

Typically, 2.5 mM $Ni(NO_3)_2{\cdot}6H_2O$, 5 mM $Co(NO_3)_2{\cdot}6H_2O$, and 15 mM hexamethylenetetramine were dissolved in 75 mL of deionized water by magnetic stirring for 30 min. Then, the solution was transferred into a 100 mL Teflon-lined stainless steel autoclave. A piece of nickel foam was immersed in the solution followed by heating of the autoclave at 95 °C for 8 h, and the top side of the nickel foam was uniformly covered with poly(tetrafluoroethylene) tape to prevent the solution contamination. After the autoclave cooled to room temperature, the Ni−Co precursor on nickel foam was washed with ethanol and deionized water several times and dried at 60 °C for 5 h. Then, the Ni−Co precursor on nickel foam was treated in a hydrothermal environment with sodium sulfide. In brief, 25 mM $Na_2S{\cdot}9H_2O$ was dissolved in 75 mL of deionized water, and then the Ni−Co precursor and solution were transferred into a 100 mL Teflon-lined stainless steel autoclave. The autoclave was heated to 120 °C for 8 h. The Ni−Co sulfide nanosheet arrays on nickel foam were obtained, washed with ethanol and deionized water, and dried at 60 °C for 5 h. For contrast, the Ni−Co oxide nanosheet arrays on nickel foam have been synthesized by annealing the Ni−Co precursor nanosheet in an air ambient atmosphere at 350 °C for 2 h with a heating rate of 1 °C min^{-1}. The average mass loadings of Ni−Co precursor, oxide, and sulfide nanosheet arrays on nickel foam were approximately 1.4, 1.2, and 2.2 mg cm^{-2}, respectively.

2.2. Asymmetric Supercapacitor Fabrication. To construct an asymmetric supercapacitor, the Ni−Co sulfide nanosheet arrays were used as the positive electrode and active carbon as the negative electrode. The negative electrode was prepared by mixing active carbon, acetylene black, and poly(vinylidene fluoride) with a mass ratio of 8:1:1, which was then pressed on nickel foam and dried at 80 °C for 12 h. The asymmetric supercapacitor was separated by a separator (NKK, MPF20AC-100), and a 2 M KOH aqueous solution was used as the electrolyte.

2.3. Material Characterization. The structures and morphologies of these samples were characterized by grazing-incident X-ray diffraction (XRD; EMPYREAN, PANalytical with Cu Kα radiation, λ = 0.15406 nm), X-ray photoelectron spectroscopy (XPS; ESCALAB 250), field-emission scanning electron microscopy (FESEM; QUANTA 400F), and high-resolution transmission electron microscopy (TEM; JEOL JEM-2010HR) with an energy-dispersive X-ray spectroscopy (EDS) detector. Nitrogen adsorption/desorption measurements were performed to investigate the surface characteristics at 77 K using a surface area analyzer (Micromeritics ASAP 2020).

2.4. Electrochemical Measurements. The nominal area of the Ni−Co oxide and Ni−Co sulfide nanosheet arrays on nickel foam immersed in the electrolyte is controlled at around 1 × 1 cm^2. The electrochemical tests were conducted with a CHI 660E electrochemical workstation (Chenhua, Shanghai) in an aqueous 2.0 M KOH electrolyte with a three-electrode cell where platinum foil serves as the counter electrode and a standard calomel electrode (SCE) as the reference electrode.

3. RESULTS AND DISCUSSION

Figure 1 illustrates the fabrication process of the Ni−Co oxide and Ni−Co sulfide nanosheet arrays on nickel foam through a two-step method. First, the Ni−Co precursor nanosheet was directly grown on nickel foam by the hydrothermal process. Then the Ni−Co oxide and Ni−Co sulfide nanosheet arrays were converted from the Ni−Co precursor nanosheet subsequently by the calcination and hydrothermal anion-exchange reaction processes, respectively. The ion-exchange reaction including cation- and anion-exchange reactions is an effective and low-cost method for chemical transformation of nanomaterials.[28−30] Nanostructured CdS, CdS-Cu_2S, and CdS-Ag_2S materials have been synthesized by a cation-exchange reaction.[31,32] The formation mechanism of Ni−Co sulfides in our work is based on an anion-exchange reaction between S^{2-} in the sodium sulfide solution and OH^- and CO_3^{2-} in the Ni−Co precursor nanosheet at hydrothermal environment. We also demonstrated that the anion-exchange reaction can take place between S^{2-} and O^{2-}, and thus the Ni−Co oxide nanosheet arrays could be converted into Ni−Co sulfide nanosheet arrays. Figure S1 in the Supporting Information (SI) shows the FESEM images of Ni−Co sulfide nanosheet arrays by anion-exchange reaction from Ni−Co oxide nanosheet arrays.

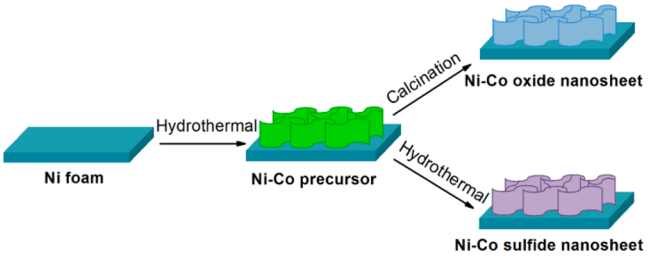

Figure 1. Schematic illustration of the fabrication process for Ni−Co precursor, oxide, and sulfide nanosheet arrays.

Figure 2 shows the typical FESEM images of the Ni−Co precursor (Figure 2a,b), oxide (Figure 2c,d,g), and sulfide

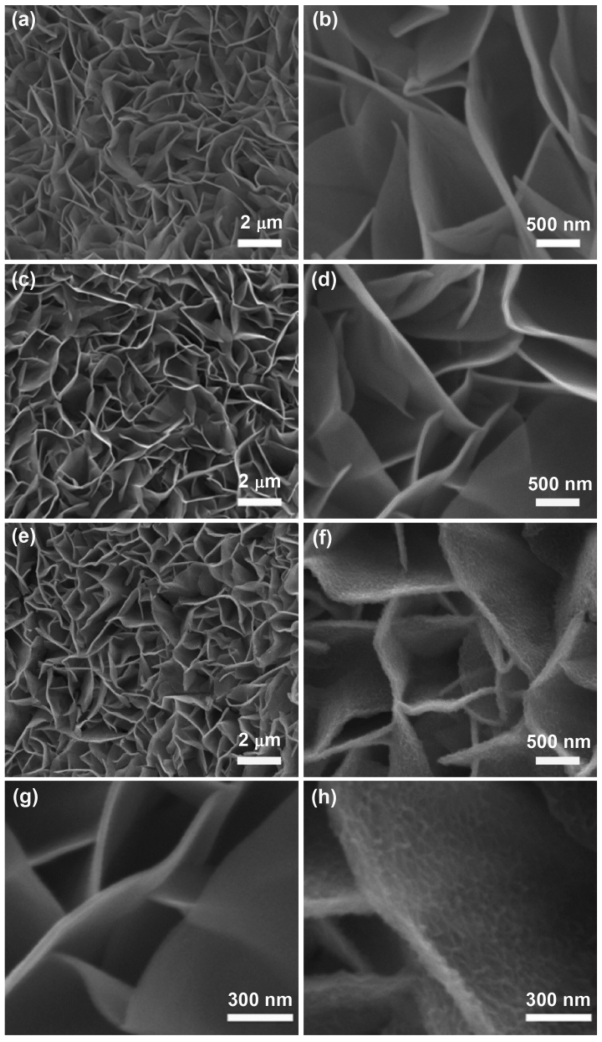

Figure 2. Typical FESEM images at different magnifications of (a and b) Ni−Co precursor nanosheet arrays, (c and d) Ni−Co oxide nanosheet arrays, (e and f) Ni−Co sulfide nanosheet arrays supported on nickel foam and (g and h) Ni−Co oxide and Ni−Co sulfide nanosheet arrays on nickel foam with high magnification, respectively.

(Figure 2e,f,h) nanosheet arrays supported on nickel foam. Obviously, the nanosheet arrays uniformly cover nickel foam, and they interconnect with each other to form a wall-like structure. As shown in Figure 2c,d, the interconnected wall-like feature of Ni−Co oxide nanosheet arrays, converted from Ni−Co precursor nanosheet arrays after thermal transformation, retained perfectly. The Ni−Co oxide nanosheet arrays have a thickness of approximately 45 nm, which is favorable for full utilization of the active materials. Meanwhile, the Ni−Co sulfide nanosheet arrays also retained the wall-like nanosheet morphology well after the hydrothermal anion-exchange reaction process. Figure S2 in the SI displays the elemental mapping images of Ni−Co sulfide nanosheet arrays on nickel foam, which indicate that the nickel, cobalt, and sulfur elements dispersed uniformly and continuously. From the high-magnification FESEM images in Figure 2g,h, there is a little difference in the morphologies between the Ni−Co oxide and sulfide nanosheet arrays. The surface of Ni−Co sulfide with a ravine-like feature is rougher than that of the Ni−Co oxide nanosheet arrays. In addition, the thickness of Ni−Co sulfide nanosheet arrays increases slightly. Through Brunauer−Emmett−Teller (BET) surface area analysis (Figure S3 in the SI), it can be seen that the BET surface area of both Ni−Co oxide (106.7 m^2 g^{-1}) and Ni−Co sulfide (22.9 m^2 g^{-1}) nanosheet arrays is higher than that of Ni−Co precursor (18.2 m^2 g^{-1}) nanosheet arrays. The huge increase of the BET surface area of Ni−Co oxide could be caused by the formation of quantities of mesopores after annealing Ni−Co precursor. The increased BET surface area of Ni−Co sulfide could be ascribed to the growth of a ravine-like surface and a few large pores after the hydrothermal anion-exchange reaction.

Figure 3a shows the XRD patterns of the Ni−Co oxide and Ni−Co sulfide nanosheet arrays on nickel foams. The two

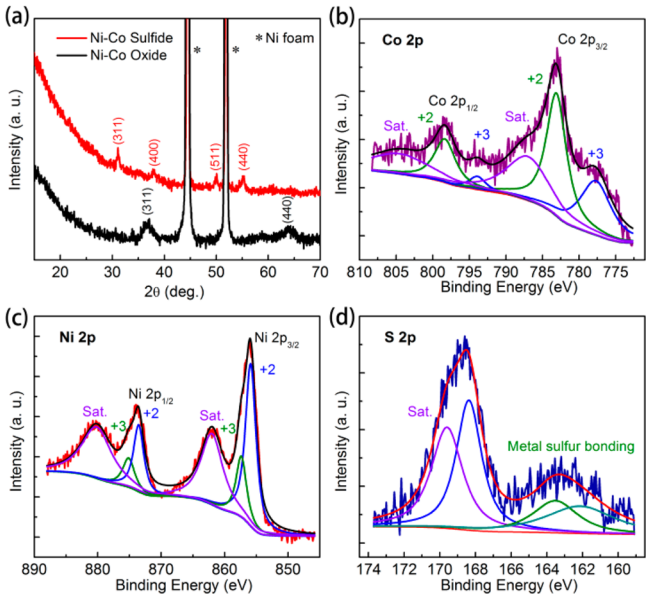

Figure 3. (a) XRD patterns of Ni−Co oxide and sulfide nanosheet arrays on nickel foam. XPS spectra of (b) Co 2p, (c) Ni 2p, and (d) S 2p for Ni−Co sulfide nanosheet arrays.

typical peaks, marked with asterisks, originate from nickel foam. Although the peaks of Ni−Co oxide nanosheet arrays are relatively weak and broad, the XRD peaks at 36° and 64°, corresponding to the (311) and (440) planes, respectively, and the selected-area electron diffraction pattern (SAED) of Ni−Co oxide nanosheet arrays (Figure S4 in the SI), indicating the (311), (400), and (620) planes, confirm the formation of the $NiCo_2O_4$ spinel phase. This result is consistent with the previous report on $NiCo_2O_4$ nanosheet arrays synthesized by a similar fabrication method.[33] The diffraction peaks of Ni−Co sulfide nanosheet arrays are also weak, indicating the low crystallinity. Four diffraction peaks at 31.4°, 38.2°, 50.1°, and 55.1°, corresponding to the (311), (400), (511), and (440) diffraction planes, respectively, can be indexed to the cubic phase of $CoNi_2S_4$ (JCPDS 24-0334) or $NiCo_2S_4$ (JCPDS 43-1477). The elemental composition and chemical state of the Ni−Co sulfide nanosheet arrays have been investigated by XPS measurements, and the corresponding results are presented in Figure 3b−d. The Co 2p and Ni 2p high-resolution spectra can be fitted with two spin−orbit doublets and two shakeup satellites (Sat.) by using a Gaussian fitting method. As shown in Figure 3b, the intensity of the Co 2p peaks is relatively weak.

The binding energies at around 777.62 and 794.13 eV of the Co 2p peaks are assigned to Co^{3+} and the binding energies at 783.25 and 798.42 eV to Co^{2+}. Likewise, in the Ni 2p spectra shown in Figure 3c, the peaks at 855.88 and 873.50 eV indicated Ni^{2+} and the peaks at 857.40 and 875.18 eV denoted Ni^{3+}. In the S 2p spectra (Figure 3d), the binding energy centered at 168.83 eV can be fitted by one main peak and one shakeup satellite peak. The peak centered at about 163.22 eV agrees with the binding energies of metal−sulfur bonding (Ni−S and Co−S bonding).[18,27,34] Therefore, the surface of the Ni−Co sulfide nanosheet arrays is composed of Co^{2+}, Co^{3+}, Ni^{2+}, Ni^{3+}, and S^{2-}. Figure S5 in the SI shows the XPS spectra of the Ni−Co oxide nanosheet arrays. The results are in accordance with the reported chemical states of $NiCo_2O_4$.[33]

The detailed morphology and structure characteristics of Ni−Co sulfide nanosheet arrays are further investigated by TEM characterization. As shown in Figure 4a,b, the surface of the Ni−Co sulfide nanosheet arrays is densely wrinkled and the planar size is about 0.8 μm, which are in good agreement with the results of FESEM images. The lattice fringes shown in Figure 4c can be indexed to the (111) crystal plane of the cubic phase. The inset of Figure 4c shows the corresponding fast Fourier transform (FFT) pattern. Simultaneously, the corresponding SAED image shown in Figure 4d implies the polycrystalline nature of Ni−Co sulfide nanosheet arrays, and the diffraction rings can be readily indexed to the (311), (400), and (440) planes of the $CoNi_2S_4$ or $NiCo_2S_4$ phase, which corresponds to the aforementioned XRD result.

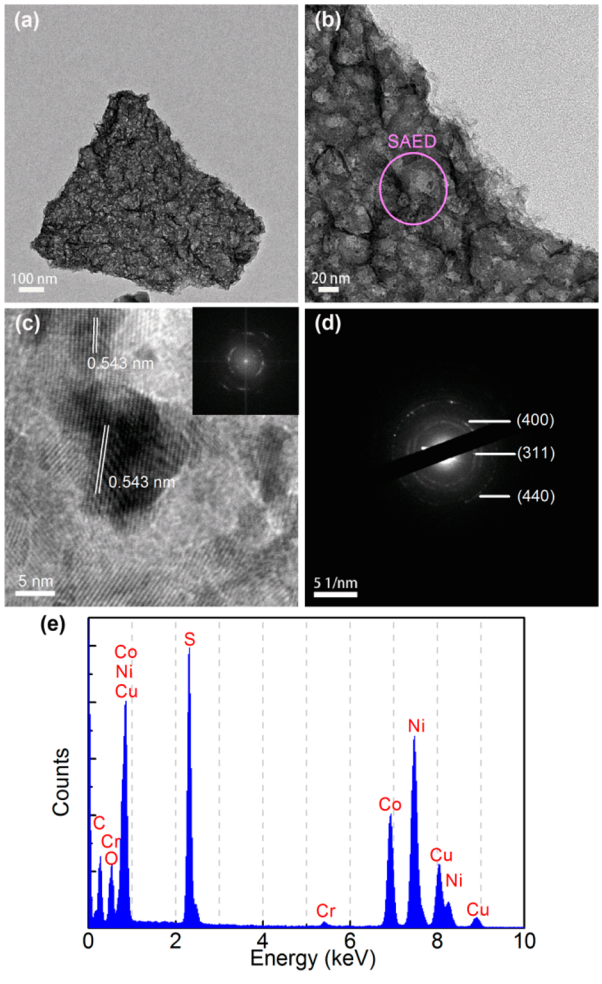

Figure 4. (a−c) TEM images of Ni−Co sulfide nanosheet arrays at different magnifications, respectively. (d) Corresponding SAED pattern of a Ni−Co sulfide nanosheet array. (e) EDS spectra of a Ni−Co sulfide nanosheet array. The inset of part c shows the corresponding FFT pattern.

In addition, EDS analysis was conducted to examine the composition of Ni−Co oxide and sulfide nanosheet arrays. The elements copper and carbon (from the TEM copper grid), chromium (from the specimen holder), nickel, cobalt, sulfur, and oxygen were detected, and the element ratio of Co/Ni/S is 1:1.85:3.5 in Ni−Co sulfide nanosheet arrays, as shown in Figure 4e. On the basis of analysis of the XRD, XPS, and TEM results, it can be identified that Ni−Co sulfide nanosheet arrays are composed of $CoNi_2S_4$ nanosheet arrays. TEM images and EDS spectra of Ni−Co oxide nanosheet arrays are shown in Figure S4 in the SI, indicating that Ni−Co oxide nanosheet arrays exhibit mesoporous structure and the element ratio of Co/Ni/ is approximately 1.15:1. Ni−Co oxide nanosheet arrays are nonstoichiometric $NiCo_2O_4$, which also implies that the Ni:Co element ratio is about 1.15:1 in Ni−Co precursor nanosheet arrays. The variation of the components and ratio of Ni/Co in Ni−Co sulfide could be attributed to the pseudo Kirkendall effect. At the beginning of hydrothermal anion-exchange reaction process, the reactions between the sulfur ions and Ni−Co precursor resulted in the formation of a ravine surface layer of Ni−Co sulfide. Then, the reactions continued by the diffusion of sulfur ions through the interface. Yin et al. have proposed that the direct conversion of the precursor core to the metal sulfide shell is therefore obstructed by the surface layer, and some previous work demonstrated that void metal sulfide nanostructures such as nanotubes and hollow nanoplates could be synthesized because of the unequal diffusion of the cobalt and sulfur ions.[13,17,29,30,34,35] However, in our study, no obvious void nanostructures but a few large pores and a changed Ni/Co element ratio of nanosheet arrays formed after anion-exchange reaction. This could be attributed to the relatively sufficient anion-exchange reaction between the Ni−Co precursor and sulfur ions because of the unique nanosheet architecture and the thin thickness of the Ni−Co precursor nanosheet. The variation of the Ni/Co element ratio, which changed from about 1:1.15 of the Ni−Co precursor to about 1.85:1 of Ni−Co sulfide, could be because the outward diffusion of the cobalt ions is much faster than the inward diffusion of the sulfur ions.[13,17,29,30,34] In addition, there might be a little reaction between nickel foam and sulfur ions.

To demonstrate the potential applications in supercapacitors, we investigated the electrochemical performance of Ni−Co precursor, oxide, and sulfide nanosheet arrays on nickel foam. Figure 5a shows the typical cyclic voltammetry (CV) curves of $CoNi_2S_4$ nanosheet arrays supported on nickel foam with the potential window from −0.1 to 0.6 V (vs SCE) at various sweep rates ranging from 3 to 20 mV s^{-1}. Clearly, the shape of the CV curves shows a pair of redox peaks during the cathodic and anodic sweeps, which is apparently distinct from the EDLCs characterized by nearly rectangular CV curves. This indicates that the capacity of $CoNi_2S_4$ nanosheet arrays results from the Faradaic redox reactions. With an increase of the sweep rates, the anodic peak current density increases and the cathodic peak current density decreases, suggesting a relatively low resistance of the electrode and fast redox reactions at the interface of the electrode and electrolyte.[36]

Figure 5b shows the galvanostatic charge−discharge (GCD) curves of $CoNi_2S_4$ nanosheet arrays on nickel foam with a

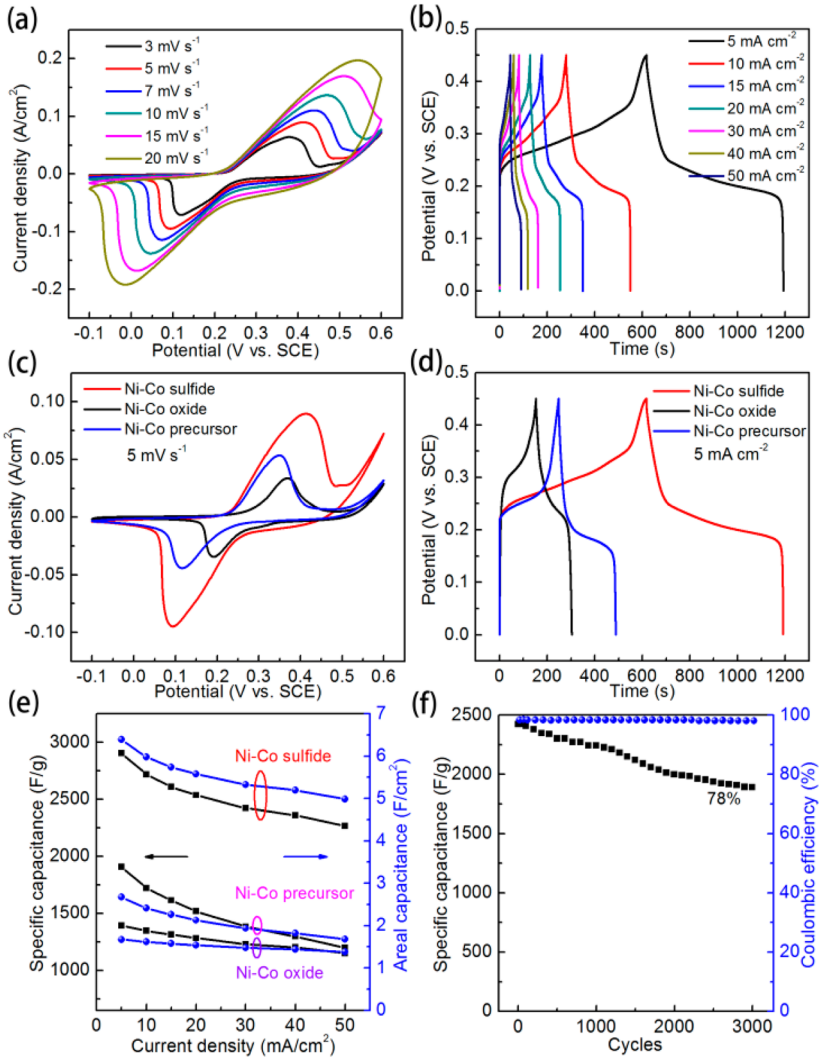

Figure 5. (a) CV curves at various scan rates and (b) GCD plots at various current densities of Ni−Co sulfide nanosheet arrays supported on nickel foam. (c) Comparative CV curves at a scan rate of 5 mV s^{-1}. (d) GCD curves at a current density of 5 mA cm^{-2} of Ni−Co precursor, oxide, and sulfide nanosheet arrays. (e) Specific capacitance and areal capacitance of Ni−Co precursor, oxide, and sulfide nanosheet arrays. (f) Cycling performance and Coulombic efficiency of Ni−Co sulfide nanosheet arrays at a current density of 30 mA cm^{-2}.

potential window of 0−0.45 V (vs SCE) at various current densities ranging from 5 to 50 mA cm^{-2}. The symmetric shape of the GCD curves implies good electrochemical capacitive characteristics and excellent reversibility of Faradaic redox reactions. The distinct plateau regions in the GCD curves demonstrate the pseudocapacitive behaviors, caused by the charge-transfer reaction and electrochemical adsorption−desorption process at the electrode/electrolyte interface, which is well consistent with the redox peaks in the CV curves. For comparison, the CV curves at a sweep rate of 5 mV s^{-1} and GCD curves at a current density of 5 mA cm^{-2} of Ni−Co precursor, oxide, and sulfide nanosheet arrays are shown in parts c and d of Figure 5, respectively. Figures S6 and S7 in the SI show the detailed CV and GCD curves of Ni−Co precursor and oxide nanosheet arrays. The CV integral area of Ni−Co sulfide is larger than that of Ni−Co precursor and oxide nanosheet arrays, and the GCD time of Ni−Co sulfide is above twice that of Ni−Co precursor and oxide nanosheet arrays at a current density of 5 mA cm^{-2}. As for the capacitance contribution of conductive substrates, the electrochemical performance of nickel foam has been investigated, as shown in Figure S8 in the SI. We agree that the capacitance contribution from nickel foam can be negligible.[15,17,37]

The specific capacitance (F g^{-1}) and areal capacitance (F cm^{-2}) of the electrode in a three-electrode system can be calculated from the galvanostatic discharge curves according to the following equation:[38,39] $C_s = I\Delta t/m\Delta V$ or $C_A = I\Delta t/S\Delta V$, where I (A), Δt (s), ΔV (V), and m (g) are designated as the current during the discharge process, the discharge time, the potential window, and the mass of active materials, respectively. The calculated specific and areal capacitance values as a function of the applied current density for Ni−Co precursor, oxide, and sulfide nanosheet arrays are shown in Figure 5e. For Ni−Co sulfide nanosheet arrays, the specific capacitance values are as high as 2906, 2719, 2609, 2538, 2423, 2362, and 2268 F g^{-1} at discharge current densities of 5, 10, 15, 20, 30, 40, and 50 mA cm^{-2}, respectively. The areal capacitances are 6.39, 5.98, 5.74, 5.58, 5.33, 5.19, and 4.99 F cm^{-2} at the corresponding current densities mentioned above. In common, as the discharge current density increases, the specific and areal capacitance values decrease gradually. This can be explained by the diffusion effect limiting the diffusion and migration of

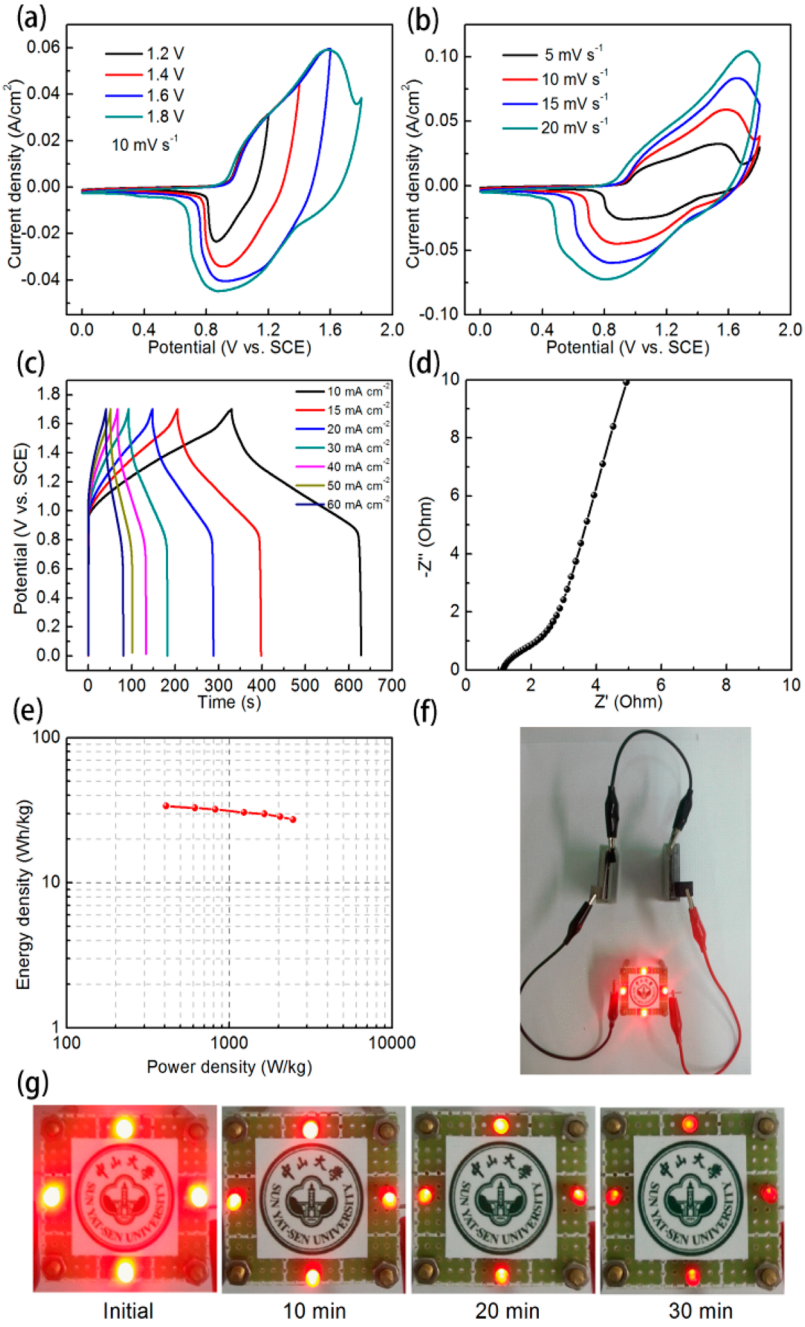

Figure 6. (a) CV curves with different scan voltage windows. (b) CV curves at various scan rates. (c) GCD plots at various current densities of the asymmetric supercapacitor cell. (d) Nyquist impedance spectra of the asymmetric supercapacitor cell. (e) Ragone plots of the asymmetric supercapacitor cell. (f) Four LEDs powered by two asymmetric supercapacitor cells in series. (g) Photographs of LEDs at different lighting times.

electrolyte ions OH^- within the electrode at a high discharge current density.[40,41] It is worth noting that Ni−Co sulfide nanosheet arrays remain at 2267 F g^{-1} (4.99 F cm^{-2}) at 50 mA cm^{-2} and hold 78.0% retention of the capacity when the rate increases from 5 to 50 mA cm^{-2}, implying good rate capability. Evidently, in our work, the specific and areal capacitance values of Ni−Co sulfide nanosheet arrays are significantly higher than those of Ni−Co precursor and oxide nanosheet arrays, and this performance is also remarkable compared with previously reported values for metal sulfide electrodes. For instance, Pu and co-workers obtained a specific capacitance of 783 F g^{-1} at a current density of 2 A g^{-1} in $NiCo_2S_4$ nanotube arrays on nickel foam.[17] Du and co-workers reported that the $CoNi_2S_4$/graphene nanocomposites possess a specific capacitance of 1652 F g^{-1} at a current density of 5 A g^{-1}.[27] Li and co-workers prepared Ni−Co sulfide nanowires on nickel foam and obtained a high specific capacitance of 2053 F g^{-1} and areal capacitance of 5.1 F cm^{-2} at a current density of 5 mA cm^{-2}.[20] Nyquist impedance spectral measurements were also carried out to evaluate the charge transfer and electrolyte diffusion in the electrode/electrolyte interface, as shown in Figure S9 in the SI. Obviously, the Nyquist impedance plots of the Ni−Co precursor, oxide, and sulfide electrodes are composed of a semicircle at the high-frequency region and a straight line at the low-frequency region. The internal and charge-transfer resistance values of these samples are almost the same at the

high-frequency region. However, according to the high slope of the straight line, the Ni−Co sulfide electrode exhibits lower diffusive resistance than the Ni−Co precursor and oxide electrodes at the low-frequency region, which could improve the diffusion and transportation of the electrolyte ions into the electrode materials.[42,43]

The superior supercapacitive performance of $CoNi_2S_4$ nanosheet arrays can be attributed to the following aspects: (1) The ravine-like nanosheet structure of $CoNi_2S_4$ nanosheet arrays is directly grown on nickel foam with good mechanical and electrical contact. (2) The ravine-like nanosheet architectures not only provide numerous electroactive sites for the adsorption of ions but also contribute efficient pathways for charge transportation.[33,36,44] (3) $CoNi_2S_4$ nanosheet arrays exhibit low crystallinity and good wettability without an annealing process, which are beneficial for improving the supercapacitive performance.[15,45,46] (4) $CoNi_2S_4$ nanosheet arrays possess higher conductivity and richer redox reaction compared to Ni−Co precursor and oxide nanosheet arrays.[16,18,20]

The cycling stability of $CoNi_2S_4$ nanosheet arrays on nickel foam as an important factor for supercapacitor application is evaluated by repeated GCD measurements at a current density of 30 mA cm^{-2}. Figure 5f shows the cycling performance and corresponding Coulombic efficiency of $CoNi_2S_4$ nanosheet arrays on nickel foam. As the cycle number increases, the specific capacitance decreases gradually. $CoNi_2S_4$ nanosheet arrays on nickel foam retain a high specific capacitance of 1889 F g^{-1} even after 3000 cycles, indicating good cycling stability. The Coulombic efficiency, calculated from the equation[47] $\eta = t_d/t_c \times 100\%$, where t_c and t_d are designated as the charge and discharge times, is about 98.5% over the entire cycling measurement, which demonstrates the excellent reversibility of $CoNi_2S_4$ nanosheet arrays.

In order to illustrate the potential application of $CoNi_2S_4$ nanosheet arrays for electrochemical energy storage, an aqueous asymmetric supercapacitor cell was assembled and measured, in which $CoNi_2S_4$ nanosheet arrays were used as the positive electrode and active carbon was used as the negative electrode with one piece of filter paper as the separator. To obtain the maximum performance of the asymmetric supercapacitor cell, the charges of the positive and negative electrodes should be optimized based on the electrochemical performance of active carbon and $CoNi_2S_4$ nanosheet arrays, as shown in Figure S10 in the SI, and the relationship[48] $m_+/m_- = C_-\Delta E_-/C_+\Delta E_+$, where C_+ and C_- represent the specific capacitance values of the positive and negative electrodes, respectively, and ΔE is the potential range. Figure 6a shows the CV curves of the asymmetric supercapacitor cell at different voltage windows in a 2 M KOH electrolyte at a scan rate of 10 mV s^{-1}. It is noted that the stable electrochemical window of the asymmetric supercapacitor cell can be extended to 1.8 V. Figure 6b shows the CV curves at various scan rates, and Figure 6c displays the GCD curves of the asymmetric supercapacitor cell at various current densities in a voltage window from 0 to 1.7 V. The GCD curves are nearly symmetrical, indicating good electrochemical capacitive characteristics and excellent reversibility of Faradaic redox reactions. Figure 6d shows the Nyquist impedance spectra of the asymmetric supercapacitor cell. It is worth noting that the charge-transfer resistance is about 1 Ω, implying that $CoNi_2S_4$ nanosheet arrays exhibit favorable charge-transfer kinetics and fast electron transport. The power and energy densities are two key parameters to characterize the performance of the electrochemical supercapacitor. Figure 6e shows the Ragone plots of the asymmetric supercapacitor cell based on the galvanostatic discharge curves. Note that the aqueous asymmetric supercapacitor cell delivers a high energy density of 33.9 Wh kg^{-1} at a power density of 409 W kg^{-1} and still maintains an energy density of 27.2 Wh kg^{-1} at a high power density of 2458 W kg^{-1}. Furthermore, two asymmetric supercapacitors in series can easily light four red-light-emitting diodes (LEDs) with a working voltage of 1.8 V more than 30 min after separate charging for a total time of 6 min, as shown in Figure 6f,g, which indicates the potential applications in supercapacitor devices.

4. CONCLUSIONS

In conclusion, we have successfully in situ grown $CoNi_2S_4$ nanosheet arrays on nickel foams through a facile two-step hydrothermal method for electrochemical energy storage. The efficient and low-cost two-step fabrication method involves the hydrothermal method and anion-exchange reaction. $CoNi_2S_4$ nanosheet arrays supported on nickel foam are able to deliver an ultrahigh specific capacitance of 2906 F g^{-1} and areal capacitance of 6.39 F cm^{-2} at a current density of 5 mA cm^{-2}, as well as good rate capability and long cycle stability in a three-electrode test system. The excellent electrochemical performance of $CoNi_2S_4$ nanosheet arrays can be attributed to a ravine-like nanosheet structure with good mechanical and electrical contact, low crystallinity and good wettability without an annealing process, rich redox reactions, as well as high conductivity and transport rate for both electrolyte ions and electrons. An asymmetric supercapacitor cell based on $CoNi_2S_4$ nanosheet arrays as the positive electrode and active carbon as the negative electrode exhibits a high energy density of 33.9 Wh kg^{-1} at a power density of 409 W kg^{-1}. Our results suggest that $CoNi_2S_4$ nanosheet arrays can find opportunity in supercapacitor applications.

■ ASSOCIATED CONTENT

Supporting Information

FESEM images of Ni−Co sulfide nanosheet arrays, elemental mapping images of Ni−Co sulfide nanosheet arrays, nitrogen adsorption/desorption isotherms of Ni−Co precursor, oxide, and sulfide nanosheet arrays, TEM images and XPS spectra of Ni−Co oxide nanosheet arrays, detailed CV and GCD curves of Ni−Co precursor and oxide nanosheet arrays, electrochemical performance of nickel foam, Nyquist impedance spectra of Ni−Co precursor, oxide, and sulfide nanosheet arrays, and CV curves of active carbon and $CoNi_2S_4$ nanosheet arrays. This material is available free of charge via the Internet at http://pubs.acs.org.

■ AUTHOR INFORMATION

Corresponding Author

*E-mail: stsbdh@mail.sysu.edu.cn.

Notes

The authors declare no competing financial interest.

■ ACKNOWLEDGMENTS

The authors gratefully acknowledge financial support from the Natural Science Foundation of China (Grant 51372281), National Basic Research Program (973 Program) of China (Grant 2012CB619302), and Program for Changjiang Scholars and Innovative Research Team in University (IRT13042).

REFERENCES

(1) Simon, P.; Gogotsi, Y.; Dunn, B. Where Do Batteries End and Supercapacitors Begin? *Science* **2014**, *343*, 1210−1211.

(2) Simon, P.; Gogotsi, Y. Materials for Electrochemical Capacitor. *Nat. Mater.* **2008**, *7*, 845−854.

(3) Wang, G. P.; Zhang, L.; Zhang, J. J. A Review of Electrode Materials for Electrochemical Supercapacitor. *Chem. Soc. Rev.* **2012**, *41*, 797−828.

(4) Zhang, L. L.; Zhao, X. S. Carbon-Based Materials as Supercapacitor Electrodes. *Chem. Soc. Rev.* **2009**, *38*, 2520−2531.

(5) Frackowiak, E. Carbon Materials for Supercapacitor Application. *Phys. Chem. Chem. Phys.* **2007**, *9*, 1774−1785.

(6) Futaba, D. N.; Hata, K.; Yamada, T.; Hiraoka, T.; Hayamizu, Y.; Kakudate, Y.; Tanaike, O.; Hatori, H.; Yumura, M.; Iijima, S. Shape-Engineerable and Highly Densely Packed Single-Walled Carbon Nanotubes and Their Application as Super-Capacitor Electrodes. *Nat. Mater.* **2011**, *5*, 987−994.

(7) Chen, H.; Zhou, S. X.; Wu, L. M. Porous Nickel Hydroxide−Manganese Dioxide-Reduced Graphene Oxide Ternary Hybrid Spheres as Excellent Supercapacitor Electrode Materials. *ACS Appl. Mater. Interfaces* **2014**, *6*, 8621−8630.

(8) Chen, H.; Hu, L. F.; Yan, Y.; Che, R. C.; Chen, M.; Wu, L. M. One-Step Fabrication of Ultrathin Porous Nickel Hydroxide−Manganese Dioxide Hybrid Nanosheets for Supercapacitor Electrodes with Excellent Capacitive Performance. *Adv. Energy Mater.* **2013**, *3*, 1636−1646.

(9) Yuan, C. Z.; Wu, H. B.; Xie, Y.; Lou, X. W. Mixed Transition-Metal Oxides: Design, Synthesis, and Energy-Related Applications. *Angew. Chem., Int. Ed.* **2014**, *53*, 1488−1504.

(10) Chen, H.; Hu, L. F.; Chen, M.; Yan, Y.; Wu, L. M. Nickel−Cobalt Layered Double Hydroxide Nanosheets for High-Performance Supercapacitor Electrode Materials. *Adv. Funct. Mater.* **2014**, *24*, 934−942.

(11) Snook, G. A.; Kao, P.; Best, A. S. Conducting-Polymer-Based Supercapacitor Devices and Electrodes. *J. Power Sources* **2011**, *196*, 1−12.

(12) Lai, C. H.; Lu, M. Y.; Chen, L. J. Metal Sulfide Nanostructures: Synthesis, Properties and Applications in Energy Conversion and Storage. *J. Mater. Chem.* **2012**, *22*, 19−30.

(13) Pu, J.; Wang, Z. H.; Wu, K. L.; Yu, N.; Sheng, E. H. Co_9S_8 Nanotube Arrays Supported on Nickel Foam for High-Performance Supercapacitors. *Phys. Chem. Chem. Phys.* **2014**, *16*, 785−791.

(14) Xia, X. H.; Zhu, C. R.; Luo, J. S.; Zeng, Z. Y.; Guan, C.; Ng, C. F.; Zhang, H.; Fan, H. J. Synthesis of Free-Standing Metal Sulfide Nanoarrays via Anion Exchange Reaction and Their Electrochemical Energy Storage Application. *Small* **2014**, *10*, 766−773.

(15) Chen, H. C.; Jiang, J. J.; Zhang, L.; Xia, D. D.; Zhao, Y. D.; Guo, D. Q.; Qi, T.; Wan, H. Z. In situ Growth of $NiCo_2S_4$ Nanotube Arrays on Ni Foam for Supercapacitors: Maximizing Utilization Efficiency at High Mass Loading to Achieve Ultrahigh Areal Pseudocapacitance. *J. Power Sources* **2014**, *254*, 249−257.

(16) Xiao, J. W.; Wan, L.; Yang, S. L.; Xiao, F.; Wang, S. Design Hierarchical Electrodes with Highly Conductive $NiCo_2S_4$ Nanotube Arrays Grown on Carbon Fiber Paper for High-Performance Pseudocapacitors. *Nano Lett.* **2014**, *14*, 831−838.

(17) Pu, J.; Wang, T. T.; Wang, H. Y.; Tong, Y.; Lu, C. C.; Kong, W.; Wang, Z. H. Direct Growth of $NiCo_2S_4$ Nanotube Arrays on Nickel Foam as High-Performance Binder-Free Electrodes for Supercapacitors. *ChemPlusChem.* **2014**, *79*, 577−583.

(18) Chen, H. C.; Jiang, J. J.; Zhang, L.; Wan, H. Z.; Qi, T.; Xia, D. D. Highly Conductive $NiCo_2S_4$ Urchin-Like Nanostructures for High-Rate Pseudocapacitors. *Nanoscale* **2013**, *5*, 8879−8883.

(19) Park, S. H.; Sun, Y. K.; Park, K. S.; Nahm, K. S.; Lee, Y. S.; Yoshio, M. Synthesis and Electrochemical Properties of Lithium Nickel Oxysulfide ($LiNiS_yO_{2-y}$) Material for Lithium Secondary Batteries. *Electrochim. Acta* **2002**, *47*, 1721−1726.

(20) Li, Y. H.; Cao, L. J.; Qiao, L.; Zhou, M.; Yang, Y.; Xiao, P.; Zhang, Y. H. Ni−Co Sulfide Nanowires on Nickel Foam with Ultrahigh Capacitance for Asymmetric Supercapacitors. *J. Mater. Chem. A* **2014**, *2*, 6540−6548.

(21) Liu, Y.; Zhang, J. N.; Wang, S. P.; Wang, K. X.; Chen, Z. M.; Xu, Q. Facilely Constructing 3D Porous $NiCo_2S_4$ Nanonetworks for High-Performance Supercapacitors. *New J. Chem.* **2014**, *38*, 4045−4048.

(22) Zhang, Y. F.; Ma, M. Z.; Yang, J.; Sun, C. C.; Su, H. Q.; Huang, W.; Dong, X. C. Shape-Controlled Synthesis of $NiCo_2S_4$ and Their Charge Storage Characteristics in Supercapacitor. *Nanoscale* **2014**, *6*, 9824−9830.

(23) Mei, L.; Yang, T.; Xu, C.; Zhang, M.; Chen, L. B.; Li, Q. H.; Wang, T. H. Hierarchical Mushroom-Like $CoNi_2S_4$ Arrays as a Novel Electrode Material for Supercapacitors. *Nano Energy* **2014**, *3*, 36−45.

(24) Yu, L.; Zhang, L.; Wu, H. B.; Lou, X. W. Formation of $Ni_xCo_{3-x}S_4$ Hollow Nanoprisms with Enhanced Pseudocapacitive Properties. *Angew. Chem., Int. Ed.* **2014**, *53*, 3711−3714.

(25) Peng, S. J.; Li, L. L.; Li, C. C.; Tan, H. T.; Cai, R.; Yu, H.; Mhaisalkar, S.; Srinvasan, M.; Ramakrishna, S.; Yan, Q. Y. In situ Growth of $NiCo_2S_4$ Nanosheets on Graphene for High-Performance Supercapacitors. *Chem. Commun.* **2013**, *49*, 10178−10180.

(26) Du, W. M.; Zhu, Z. Q.; Wang, Y. B.; Liu, J. N.; Yang, W. J.; Qian, X. F.; Pang, H. One-Step Synthesis of $CoNi_2S_4$ Nanoparticles for Supercapacitor Electrodes. *RSC Adv.* **2014**, *4*, 6998−7002.

(27) Du, W. M.; Wang, Z. Y.; Zhu, Z. Q.; Hu, S.; Zhu, X. Y.; Shi, Y. F.; Pang, H.; Qian, X. F. Facile Synthesis an Superior Electrochemical Performances of $CoNi_2S_4$/Graphene Nanocomposite Suitable for Supercapacitor Electrodes. *J. Mater. Chem. A* **2014**, *2*, 9613−9619.

(28) Dloczik, L.; Konenkamp, R. Nanostructure Transfer in Semiconductors by Ion Exchange. *Nano Lett.* **2003**, *3*, 651−653.

(29) Wang, Z. H.; Pan, L.; Hu, H. B.; Zhao, S. P. Co_9S_8 Nanotubes Synthesized on The Basis of Nanoscale Kirkendall Effect and Their Magnetic and Electrochemical Properties. *CrystEngComm* **2010**, *12*, 1899−1904.

(30) Fan, H. J.; Knez, M.; Scholz, R.; Nielsch, K.; Pippel, E.; Hesse, D.; Zacharias, M.; Gossele, U. Monocrystalline Spinel Nanotube Fabrication Based on The Kirkendall Effect. *Nat. Mater.* **2006**, *5*, 627−633.

(31) Sadtler, B.; Demchenko, D. O.; Zheng, H. M.; Hughes, S. M.; Merkle, M. G.; Dahmen, U.; Wang, L. W.; Alivisatos, A. P. Selective Facet Reactivity during Cation Exchange in Cadmium Sulfide Nanorods. *J. Am. Chem. Soc.* **2009**, *131*, 5285−5293.

(32) Robinson, R. D.; Sadtler, B.; Demchenko, D. O.; Erdonmez, C. K.; Wang, L. W.; Alivisatos, A. P. Spontaneous Superlattice Formation in Nanorods Through Partial Cation Exchange. *Science* **2007**, *317*, 355−358.

(33) Zhang, G. Q.; Lou, X. W. General Solution Growth of Mesoporous $NiCo_2O_4$ Nanosheets on Various Conductive Substrates as High-Performance Electrodes for Supercapacitors. *Adv. Mater.* **2013**, *25*, 976−979.

(34) Pu, J.; Cui, F. L.; Chu, S. B.; Wang, T. T.; Sheng, E. R.; Wang, Z. H. Preparation and Electrochemical Characterization of Hollow Hexagonal $NiCo_2S_4$ Nanoplates as Pseudocapacitor Materials. *ACS Sustainable Chem. Eng.* **2014**, *2*, 809−815.

(35) Wang, W. S.; Dahl, M.; Yin, Y. D. Hollow Nanocrystals through the Nanoscale Kirkendall Effect. *Chem. Mater.* **2013**, *25*, 1179−1189.

(36) Yuan, C. Z.; Li, J. Y.; Hou, L. R.; Zhang, X. G.; Shen, L. F.; Lou, X. W. Ultrathin Mesoporous $NiCo_2O_4$ Nanosheets Supported on Ni Foam as Advanced Electrodes for Supercapacitors. *Adv. Mater.* **2012**, *22*, 4592−4597.

(37) Xu, K. B.; Li, W. Y.; Liu, Q.; Li, B.; Liu, X. J.; An, L.; Chen, Z. G.; Zou, R. J.; Hu, J. Q. Hierarchical Mesoporous $NiCo_2O_4$@MnO_2 Core−Shell Nanowire Arrays on Nickel Foam for Aqueous Asymmetric Supercapacitors. *J. Mater. Chem. A* **2014**, *2*, 4795−4802.

(38) Meher, S. M.; Rao, G. R. Ultralayered Co_3O_4 for High-Performance Supercapacitor Applications. *J. Phys. Chem. C* **2011**, *115*, 15646−15654.

(39) Liu, J.; Jiang, J.; Cheng, C.; Li, H.; Zhang, J.; Gong, H.; Fan, H. J. Co_3O_4 Nanowire@MnO_2 Ultrathin Nanosheet Core/Shell Arrays: A New Class of High-Performance Pseudocapacitive Materials. *Adv. Mater.* **2011**, *23*, 2076−2081.

(40) Jiang, H.; Zhao, T.; Li, C. Z.; Ma, J. Hierarchical Self-Assembly of Ultrathin Nickel Hydroxide Nanoflakes for High-Performance Supercapacitors. *J. Mater. Chem.* **2011**, *21*, 3818−3823.
(41) Liu, B.; Liu, B. Y.; Wang, Q. F.; Wang, X. F.; Xiang, Q. Y.; Chen, D.; Shen, G. Z. New Energy Storage Option: Toward $ZnCo_2O_4$ Nanorods/Nickel Foam Architectures for High-Performance Supercapacitors. *ACS Appl. Mater. Interfaces* **2013**, *5*, 10011−10017.
(42) Niu, L. Y.; Li, Z. P.; Xu, Y.; Sun, J. F.; Hong, W.; Liu, X. H.; Wang, J. Q.; Yang, S. R. Simple Synthesis of Amorphous $NiWO_4$ Nanostructure and Its Application as a Novel Cathode Material for Asymmetric Supercapacitors. *ACS Appl. Mater. Interfaces* **2013**, *5*, 8044−8052.
(43) Pu, J.; Tong, Y.; Wang, S. B.; Sheng, E. R.; Wang, Z. H. Nickel−Cobalt Hydroxide Nanosheets Arrays on Ni Foam for Pseudocapacitor Applications. *J. Power Sources* **2014**, *250*, 250−256.
(44) Liu, X. Y.; Shi, S. J.; Xiong, Q. Q.; Li, L.; Zhang, Y. J.; Tang, H.; Gu, C. D.; Wang, X. L.; Tu, J. P. Hierarchical $NiCo_2O_4$@$NiCo_2O_4$ Core/Shell Nanoflake Arrays as High-Performance Supercapacitor Materials. *ACS Appl. Mater. Interfaces* **2013**, *5*, 8790−8795.
(45) Xu, J.; Wang, Q. F.; Wang, X. W.; Xiang, Q. Y.; Liang, B.; Chen, D.; Shen, G. Z. Flexible Asymmetric Supercapacitors Based upon Co_9S_8 Nanorod//Co_3O_4@RuO_2 Nanosheet Arrays on Carbon Cloth. *ACS Nano* **2013**, *7*, 5453−5462.
(46) Li, H. B.; Yu, M. H.; Wang, F. X.; Liu, P.; Liang, Y.; Xiao, J.; Wang, C. X.; Tong, Y. X.; Yang, G. W. Amorphous Nickel Hydroxide Nanospheres with Ultrahigh Capacitance and Energy Density as Electrochemical Pseudocapacitor Materials. *Nat. Commun.* **2013**, *4*, 1894.
(47) Wang, W. J.; Hao, Q. L.; Lei, W.; Xia, X. F.; Wang, X. Ternary Nitrogen-Doped Graphene/Nickel Ferrite/Polyaniline Nanocomposites for High-Performance Supercapacitors. *J. Power Sources* **2014**, *269*, 250−259.
(48) Fan, Z. J.; Yan, J.; Wei, T.; Zhi, L. J.; Ning, G. Q.; Li, T. Y.; Wei, F. Asymmetric Supercapacitors Based on Graphene/MnO_2 and Activated Carbon Nanofiber Electrodes with High Power and Energy Density. *Adv. Funct. Mater.* **2011**, *21*, 2366−2375.